

Exploring Parameter Redundancy in the Unitary Coupled-Cluster Ansatz for Hybrid Variational Quantum Computing

Shashank G Mehendale,^{1, a)} Bo Peng,^{2, b)} Niranjana Govind,² and Yuri Alexeev³

¹⁾*Indian Institute of Science Education and Research (IISER), Kolkata, West Bengal 741246, India*

²⁾*Physical and Computational Sciences Directorate, Pacific Northwest National Laboratory, Richland, WA 99354, United States*

³⁾*Computational Science Division, Argonne National Laboratory, Lemont, IL 60439, United States*

(Dated: April 7, 2023)

One of the commonly used chemically-inspired approaches in variational quantum computing is the unitary coupled-cluster (UCC) ansätze. Despite being a systematic way of approaching the exact limit, the number of parameters in the standard UCC ansätze exhibits unfavorable scaling with respect to the system size, hindering its practical use on near-term quantum devices. Efforts have been taken to propose some variants of UCC ansätze with better scaling. In this paper we explore the parameter redundancy in the preparation of unitary coupled-cluster singles and doubles (UCCSD) ansätze employing spin-adapted formulation, small amplitude filtration, and entropy-based orbital selection approaches. Numerical results of using our approach on some small molecules have exhibited a significant cost reduction in the number of parameters to be optimized and in the time to convergence compared with conventional UCCSD-VQE simulations. We also discuss the potential application of some machine learning techniques in further exploring the parameter redundancy, providing a possible direction for future studies.

I. INTRODUCTION

The variational quantum eigensolver (VQE) has arguably emerged as one of the most promising algorithms for the ground state estimation of molecular Hamiltonians in the noisy intermediate-scale quantum (NISQ) era. VQE starts with a given Hamiltonian and a parameterized ansatz state. The expectation value of the Hamiltonian with respect to the ansatz is taken to be the cost function that is minimized by varying the parameters of the ansatz. The task assigned to the quantum computer is to estimate the expectation value, while the task assigned to the classical computer is to predict the new parameter values based on the old expectation value. In this sense, they together form the minimization routine and hence form a quantum-classical hybrid algorithm appropriate for the NISQ era.

The first VQE experiment by Peruzzo and co-workers¹ utilized the unitary coupled-cluster singles and doubles (UCCSD) ansatz derived from unitary coupled-cluster theory^{2–10}. The standard UCCSD ansatz has an unfavorable scaling of the number of parameters with respect to the system size¹¹, which translates to a large number of quantum gates and a long circuit in the quantum simulations. The errors in these quantum gates and circuits can quickly accumulate in the simulation, hindering the practical use of the UCCSD ansatz for simulating large quantum systems on near-term quantum devices.

To prepare ansätze with favorable scaling, researchers have proposed many approaches (see Refs. 12,13 for recent reviews). Usually, the ansätze are classified into hardware-efficient type and chemically-inspired type with either fixed or adaptive structures. Hardware-efficient ansätze are flexible and easy to implement with the current quantum hard-

ware^{14,15} but suffer from so-called barren plateaus in the variational parameter landscape¹⁶ and require extra work to enforce the physical symmetries. The chemically-inspired ansätze, on the other hand, are usually focused on some UCC variants with improved scaling. Typical UCC variants with fixed circuit structures include the unitary pair coupled cluster with generalized singles and doubles (k -UpCCGSD) method¹⁷ that provides “linear” scaling with the system size while including an unknown prefactor k that needs to be determined heuristically, the orbital-optimized unitary coupled-cluster (OO-UCC) ansatz¹⁸ introducing Brueckner-type orbitals with slight performance improvement, and the double unitary coupled-cluster (DUCC) ansatz^{19,20} naturally enabling the support for more realistic active space approximations.

Between the chemically-inspired and hardware-efficient ansätze there also exists the so-called qubit coupled-cluster (QCC) method introduced by Ryabinkin et al.²¹ resembling the coupled-cluster structure but working directly with Pauli strings in the qubit space to reduce the number of two-qubit gates and pursue the efficient use of quantum resources. In practice, however, since the number of Pauli string candidates for the QCC ansätze have an exponential scaling ($\mathcal{O}(4_q^N)$, with N_q the number of qubits employed), QCC also requires a robust selection process based on an efficient estimate of the contribution of the corresponding entanglers of these Pauli strings to the correlation energy. Regarding chemically-inspired ansätze with adaptive circuit structures, typical developments include the adaptive derivative-assembled pseudo-Trotter ansatz variational quantum eigensolver (ADAPT-VQE)²², the qubit-excitation-based adaptive VQE (QEB-ADAPT-VQE)²³, the iterative QCC approach²⁴, the unitary selective coupled-cluster approach²⁵, sparse UCC ansatz²⁶, and their extensions. The key idea here is to construct an ansatz that can recover most of the correlation energy with the least number of operators and variational parameters, and the

^{a)}Electronic mail: sgm18ms074@iiserkol.ac.in

^{b)}Electronic mail: peng398@pnnl.gov

importance of the operators is typically measured through the energy gradient with respect to the corresponding variation parameters or simply their associate correlation energy contribution.

In this paper we employ other approaches to explore the interconnections between the parameters in the UCC ansätze that would possibly lead to a performance improvement in the UCC ansatz preparation. In particular, we employ spin adaption, small amplitude filtration, and entropy-based orbital selection techniques in the UCCSD framework to explore parameter redundancy. We also discuss the feasibility of applying machine learning techniques in discovering parameter redundancy. The rest of this paper is organized as follows. In Section II we give an introduction to the theoretical background and numerical methodology. In Section III we present some numerical results and the performance of our proposed UCC-VQE approaches for the quantum simulations of some prototype molecular systems. In Section IV we discuss some possible further improvements in this direction. In Section V we summarize our conclusions and briefly present ideas for future work.

II. THEORY AND METHOD

A. Unitary coupled-cluster variational quantum eigensolver

The UCC ansatz entails a unitary evolution of starting state formed by an exponential parameterization of the wavefunction. The unitary evolution is implemented on a quantum computer using a set of one and two-qubit gates. For molecular systems, the cluster operator consists of all the excitation operators from the occupied orbitals to the virtual orbitals, which, when acting on the single reference state, produces a linear combination of all possible excited determinants. In practice, the cluster operator is usually truncated to singles, doubles, or a few more excitations. In this work we mainly use the UCCSD approach. The reference state is usually taken to be the Hartree–Fock state of the molecular system, $|\text{HF}\rangle$. Hence a parametrized UCC ansatz is given by

$$|\psi(\vec{\theta})\rangle = e^{\mathbf{T}(\vec{\theta}) - \mathbf{T}^\dagger(\vec{\theta})} |\text{HF}\rangle, \quad (1)$$

where for a UCCSD ansatz we have

$$\mathbf{T}(\vec{\theta}) = \sum_{i,a} t_i^a(\vec{\theta}) a_a^\dagger a_i + \sum_{i<j,a<b} t_{ij}^{ab}(\vec{\theta}) a_a^\dagger a_b^\dagger a_j a_i, \quad (2)$$

with i, j, \dots being occupied spin orbital indices and a, b, \dots being virtual spin orbital indices. Here t_i^a, t_{ij}^{ab} are the single and double cluster amplitudes. The task of VQE is then to provide the minimum value of the expectation value of the Hamiltonian H with respect to the parameterized state as

$$E = \min_{\vec{\theta}} \langle \psi(\vec{\theta}) | H | \psi(\vec{\theta}) \rangle. \quad (3)$$

B. Spin-adapted unitary coupled cluster

The first parameter simplification method we employ in this work is the well-known technique of spin adaption^{27,28}. In a typical UCC-VQE minimization, each parameter of the excitation operator is treated as an independent variable. Thus, the resulting state from the minimization need not be an eigenstate of the total spin, S^2 , operator. In many cases, however, we expect the ground state of the Hamiltonian to be an eigenstate of the S^2 operator. Hence, in order to make sure that we do not break the spin-symmetry, some conditions on the excitation operators can be used. These ensure that the cluster operator commutes with the S^2 operator and hence leads to an eigenstate of the total spin. Consequently, the number of independent cluster amplitudes is considerably reduced. In Eq. (2), if we relabel the subscripts of cluster amplitudes to mean occupied/virtual spatial orbitals instead of spin orbitals and specifically mention the flavor of the spin (α, β) besides these indices, then the spin adaption relations of a closed shell electron configuration can be given as

$$t_{i\alpha}^{\alpha\alpha} = t_{i\beta}^{\alpha\beta} \quad (4)$$

$$t_{i\alpha j\alpha}^{\alpha\alpha b\alpha} = t_{i\beta j\beta}^{\alpha\beta b\beta} = t_{i\alpha j\beta}^{\alpha\alpha b\beta} + t_{i\alpha j\beta}^{\alpha\beta b\alpha} \quad (5)$$

$$t_{i\alpha j\beta}^{\alpha\alpha b\beta} = t_{i\beta j\alpha}^{\alpha\beta b\alpha} \quad \& \quad t_{i\alpha j\beta}^{\alpha\beta b\alpha} = t_{i\beta j\alpha}^{\alpha\alpha b\beta}. \quad (6)$$

However, as has been noted in the literature²⁹, this procedure reduces only the number of independent parameters supplied to the classical part of the UCC-VQE routine and does not reduce the number of quantum gates and the circuit depth. We also mention that even though we could implement these restrictions to preserve spin symmetry, in a practical implementation we would have to resort to Trotter decomposition, which might actually induce additional errors and hence break the symmetry if the Trotter error is not well controlled²⁹. We will use the spin-adapted UCCSD or its notation SA-UCCSD interchangeably in this paper.

C. Single orbital entropy

Another important concept used in this work is the single orbital entropy³⁰. The von Neumann entropy of a system that is represented by a density matrix ρ is given by

$$S = -\rho \ln \rho = -\sum_i \lambda_i \ln \lambda_i, \quad (7)$$

where λ_i is the i th eigenvalue of the density matrix. For a pure state, the value of the entropy is zero, while for the maximally mixed state, the value of the entropy is maximum. Calculation of entropy is useful for evaluating the amount of entanglement in a system, and it is done by measuring what is known as the entanglement entropy. Given a pure state of a system with two subsystems A and B , the entanglement entropy is defined as the von Neumann entropy of the reduced density matrices of either of the subsystems.

Writing the electronic ground state as a density matrix, we can take any of the molecular orbitals as a single subsystem and the remaining orbitals as another subsystem

and calculate the entanglement entropy of this molecular orbital. This calculation gives the amount of entanglement shared between the single molecular orbital and the rest of the molecular orbitals. This entropy for each of the orbitals is called the single-orbital entropy. Mathematically, let $|\psi\rangle$ be the ground state of the Hamiltonian in the Fock space

$$|\psi\rangle = \sum_{n_1, n_2, \dots} N_{n_1, n_2, \dots} |n_1, n_2, \dots\rangle, \quad (8)$$

where n_i corresponds to the occupation of the i th spatial orbital. That is, n_i can take one value from the set $\{-, \uparrow, \downarrow, \uparrow\downarrow\}$ corresponding to a possible occupation state: no electron, only α electron, only β electron, and both α and β electrons, respectively. The corresponding density matrix will be

$$\rho = \sum_{\substack{n_1, n_2, \dots \\ n'_1, n'_2, \dots}} N_{n_1, n_2, \dots} |n_1, n_2, \dots\rangle \langle n'_1, n'_2, \dots| N^*_{n'_1, n'_2, \dots} \quad (9)$$

Then, for example, the reduced density matrix of the first spatial orbital can be calculated as

$$\rho_1 = \sum_{\substack{n''_2, n''_3, \dots \\ n'_1, n'_2, \dots}} \sum_{\substack{n_1, n_2, \dots \\ n'_1, n'_2, \dots}} N_{n_1, n_2, \dots} \langle n''_2, n''_3, \dots | n_1, n_2, \dots \rangle \times \langle n'_1, n'_2, \dots | n''_2, n''_3, \dots \rangle N^*_{n'_1, n'_2, \dots} \quad (10)$$

Given that both n_1 and n'_1 can take four different values, ρ_1 will be a 4×4 matrix. From this, we can calculate the entanglement entropy or single-orbital entropy of the first spatial orbital as

$$S_1 = -\rho_1 \ln \rho_1 = -\sum_{i=1}^4 \lambda_i \ln \lambda_i, \quad (11)$$

where λ_i is the i th eigenvalue of the reduced density matrix ρ_1 . The value of S_1 is a measure of entanglement between the first spatial orbital and the rest of the orbitals. For example, it is zero when the first orbital can be separated from all the others in Eq. (8). Single-orbital entropy and/or the mutual information are usually employed as a diagnostic measure of the correlation for the active space selection in the complete active space calculations or system partitioning in the quantum embedding calculations^{31–33}. In this work we propose a way to utilize the single-orbital entropy values to conduct orbital selection for correlation energy calculation.

D. Numerical approach

Our proposed UCC-VQE numerical approach consists of three parts: spin adaption, small amplitude filtration, and entropy-based orbital selection. The aim is to minimize the computational cost of the conventional UCC-VQE simulation through exploring and removing the redundancy in the parameter space of the UCC ansatz. Spin adaption was briefly introduced above. The details of the other two techniques used in our algorithm are explained below.

If a certain portion of the parameters stays negligibly small throughout the minimization procedure, then the corresponding excitations can be heuristically identified from

the first κ (κ is a small integer and $\kappa_{\min} = 2$) iterations of the UCC-VQE approach and removed afterward. We denote this approach as small amplitude filtration (SAF). We combine this technique with spin adaption in the UCC-VQE approach to have a more efficient UCC-VQE variant (denoted SA-SAF-UCC-VQE). The SA-SAF-UCC-VQE procedure can be described as follows.

1. Perform conventional UCC-VQE for κ iterations.
2. Apply two conditions on the parameters obtained from the $(\kappa - 1)$ th and κ th iterations: (1) the absolute values of the parameters at the κ th iteration, $|\vec{\theta}|$, need to be smaller than a small cutoff ϵ_1 and (2) the absolute value of the change in the parameter values from the $(\kappa - 1)$ th to the κ th iteration, $|\Delta\vec{\theta}|$, needs to be smaller than another small cutoff ϵ_2 .
3. Eliminate the parameters that satisfy conditions (1) and (2), remove the corresponding gates from the circuit, and keep optimizing the remaining parameters.

The resulting reduction in the number of parameters and execution time is observed to be significant. Remarkably, the κ is a heuristic small integer that represents the number of full UCCSD iterations needed to detect small UCCSD amplitudes. Also, the first κ full UCCSD iterations can be run either on the classical side or on the quantum computer. If they are run on the quantum computer, the circuit depth for the VQE-UCCSD run remains the same. However, after the small amplitude filtration, the UCCSD ansatz will have a shallower circuit compared to the full UCCSD ansatz. As will be shown in Section III, removing the small amplitude can significantly accelerate the convergence, as subsequent iterations will require fewer parameters.

Regarding the entropy-based orbital selection, we want to screen out the orbitals that have a significantly lower entropy value, and correspondingly negligible contributions to the total correlation, in comparison with other orbitals. The efficiency of the UCC-VQE simulation can then be improved by freezing these orbitals in the Hamiltonian to obtain an approximate yet sufficiently accurate correlation energy for the whole system. Since the orbital selection is based on the ordering of the orbital entropy values and their relative discrepancy, the approximate reduced density matrices obtained from some low-level correlation approaches can be sufficient for the entropy calculations. In this sense, without explicitly mentioning it, the reduced density matrices are computed at both Møller–Plesset (MP2) and CCSD levels in the present study.

III. NUMERICAL RESULTS

We applied the SA-SAF-UCCSD-VQE approach for computing the ground state energies of five molecular systems— H_4 (Linear), H_4 (Ring), H_6 , LiH, and H_2O —in the STO-3G basis. We used the Qskit³⁴ module in Python to implement our proposed approach. The *aer_simulator_statevector* backend was used to perform the quantum computing emulation.

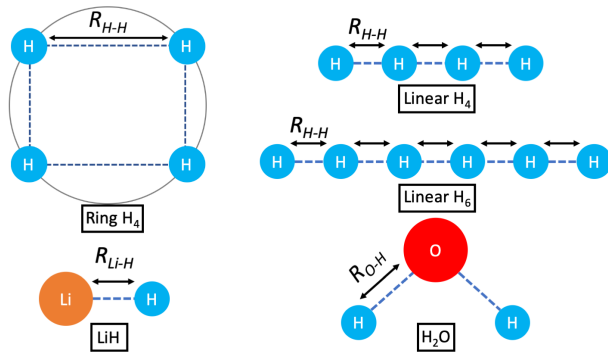


Figure 1. Five molecular systems with varying bond lengths were studied in this work. The H-O-H angle in H_2O is fixed to be 104.5° .

We will first explain the structures of the molecules considered. Next, we will show the robustness of the SAF by comparing the number of free parameters in the excitation operator and the time to convergence in the UCCSD-VQE ground state simulations of the five molecules with and without employing spin adaption and/or small amplitude filtration. Then, we will show the accuracy of the algorithm by comparing the converged energy for each of the three algorithms presented here. After that, we will discuss the improvement offered by the entropy calculations.

For each of the molecules discussed below, unless mentioned otherwise, the SciPy³⁵ minimizer *L-BFGS-B* has been used for the classical minimization routine that constitutes the classical part of the UCC-VQE algorithm. The initial parameter values for all the amplitudes of the ansatz have been chosen to be zero. The Hartree-Fock state has been used as the reference for the ansatz. The Jordan-Wigner³⁶ transformation is employed to convert Fermionic operators to Pauli operators.

A. Molecular Structures

Five molecular systems, namely ring and linear H_4 , linear H_6 , LiH , and H_2O molecules, with varying bond lengths are employed for numerical tests in this work. In all the calculations, STO-3G basis were used which generates 8, 12, 12, and 14 spin orbitals for H_4 , H_6 , LiH , H_2O molecules, respectively.

B. Performance of SA-SAF-UCCSD-VQE

To understand the improvement offered by spin adaption and small amplitude filtration, we first look at the number of free parameters reduced by employing these schemes in the UCCSD-VQE approach and the time to convergence in the ground state simulations of the five molecules. We collected the number of free parameters required in three approaches UCCSD-VQE, SA-UCCSD-VQE, SAF-UCCSD-VQE, and SA-SAF-UCCSD-VQE. The comparison is given in Fig. 2a. As can be seen, compared with the conventional UCCSD-VQE, the application of spin adaption or small amplitude

filtration can reduce the number of parameters in the optimization by roughly half; and combining both spin adaption and small amplitude filtration as in SA-SAF-UCCSD-VQE further reduces the number of free parameters to be only roughly one-quarter of that in the conventional UCCSD-VQE. Since the number of parameters that need to be optimized is greatly reduced, the VQE execution time is also significantly reduced. As shown in Fig. 2b, as the system size grows and bond length elongates (the latter usually indicates the electron correlation gets stronger), the time saved by combining spin adaption and small amplitude filtration is more significant than that by employing only spin adaption in the UCCSD-VQE approach. We mention that in the SA-SAF-UCCSD-VQE simulations, we set $\kappa = \kappa_{\min} = 2$. It is worth mentioning that the term “time” in Figure 2b refers to the actual amount of time taken by the UCCSD-VQE approaches employing a quantum emulator running on a classical machine. This is associated with the difference in the time taken for each iteration and the number of iterations for different UCCSD-VQE approaches studied in this work. Since our simulator does not take noise and shot count into account, the “time” is not a quantitative measure of the actual duration of these approaches when running on a real quantum machine. However, the “time” values shown in Figure 2b are still a good measure of the time taken by the classical routine of VQE. Hence, one of the major advantages of SA-SAF-UCCSD-VQE is the reduction of time taken by the classical routine of VQE.

Figure 3 shows the average values of the amplitudes (identified as the small amplitudes after $\kappa = 2$ UCCSD-VQE iterations) at the end of the UCCSD-VQE simulations of the five molecules at different bond lengths. As can be seen, the average values of the small amplitudes at the end of the UCCSD-VQE simulations remain mostly less than 10^{-5} throughout the bond length range, indicating that these small amplitudes are relatively independent of the evolution of the primary amplitudes, and their changes and impact on the minimization are trivial.

Regarding the reduction of quantum resources using the proposed approach, it is worth noting that (1) only small amplitude filtration and/or entropy-based orbital selection (as will be discussed later) can help reduce the number of CNOT gates and the circuit depth in the UCCSD ansatz, (2) the UCCSD ansatz typically requires Trotterization, which involves decomposing the product into a series of exponentials of single and double UCC operators, to facilitate implementation in a quantum circuit. The exponential of a UCC single operator is a Givens rotation³⁷, and its simplified circuit for adjacent two qubits requires only two CNOT gates³⁸. The exponential of a UCC double operator can be encoded using a fermionic- (FEB) and qubit-excitation-based (QEB) circuit structures^{39,40}, and (3) since the indices in the single and double UCC operators are not necessarily adjacent to each other, one would need to use the fermionic SWAP (f-SWAP) gate⁴¹ to make them adjacent. An f-SWAP gate can be decomposed as a sequence of a Control-Z gate and three CNOT gates, and for two fermionic modes separated by a distance of d , $3d$ CNOT gates are usually required to perform the f-SWAP operation. Taking all these factors into account, Figure 4, for example, shows the number of CNOT gates and the circuit depth of

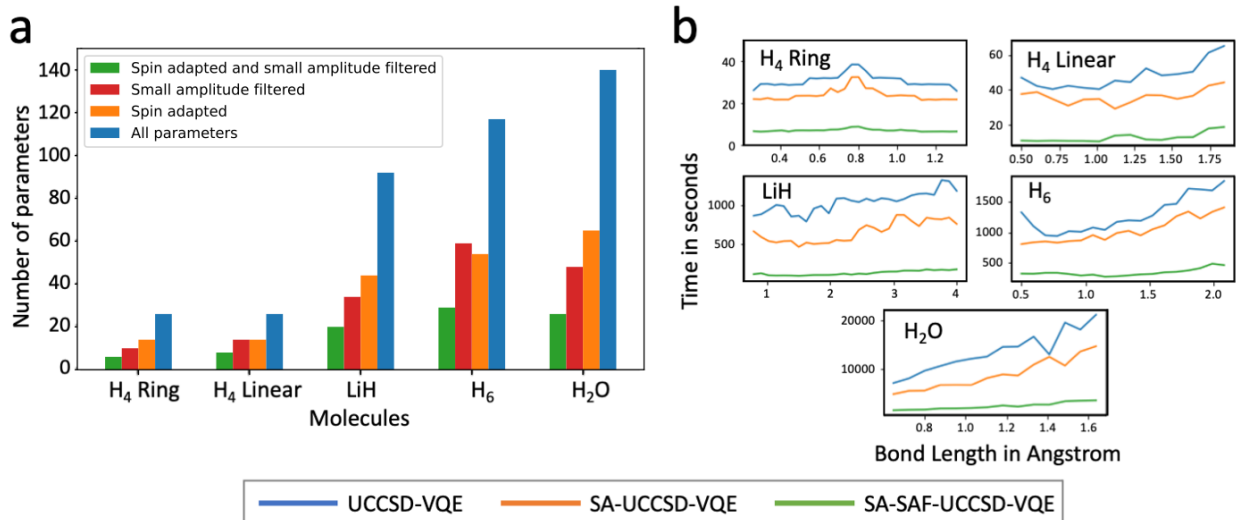


Figure 2. Performance of the UCCSD-VQE (blue), SA-UCCSD-VQE (orange), and SA-SAF-UCCSD-VQE (green) approaches for obtaining the ground states of five molecules in terms of (a) the number of the parameters and (b) the time to convergence (after removing small amplitudes for the case of SA-SAF-UCCSD-VQE). Number of parameters requirement employing only small amplitude filtration in UCCSD-VQE is also included in (a) for comparison. In the SA-SAF-UCCSD-VQE approach, we set $\kappa = 2$, $\epsilon_1 = 10^{-4}$, and $\epsilon_2 = 10^{-5}$. In all the UCCSD-VQE calculations, the convergence is reached when the energy variant is less than 10^{-6} a.u.

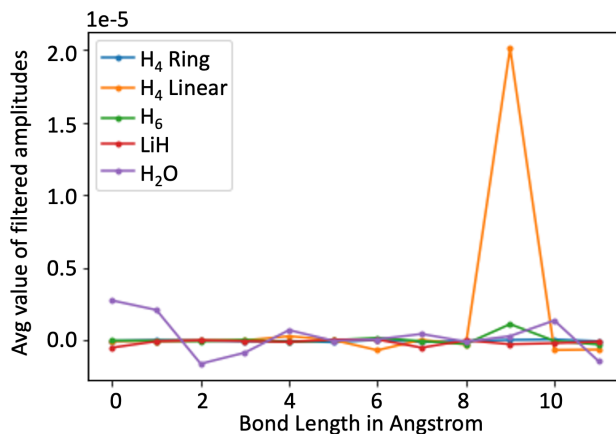


Figure 3. Average values of the small amplitudes at the end of UCCSD-VQE simulations of the five molecules at different bond lengths. Each molecule is scanned over a range of bond lengths that have been discretized to 12 bond length indices.

the UCCSD ansatz before and after small amplitude filtration. Similar to Figure 2, more than a 50% reduction can be observed for all test cases.

We further compare the potential energy surfaces (PES's) computed by different UCCSD-VQE noise-free simulations discussed here, as well as by the exact diagonalization. The results are shown in Fig. 5. As can be seen, the error in energy compared in columns two and three of the figures are considerably small. Looking more closely at the extent of overlap, we see that the second column of Fig. 5 shows the error between the UCCSD-VQE energies and the SA-UCCSD-VQE energies, and the third column shows the error between the SA-UCCSD-VQE energies and SA-SAF-UCCSD-VQE energies. We can clearly see that all the errors are extremely small (with the highest being on the order of 10^{-5} for H₂O), proving that removing the small amplitudes makes a negligible difference in the converged energies as compared with the approach that retains these

amplitudes, and the small amplitude filtering is reliable for calculating the ground states of the studied molecules. We mention that the small amplitude filtering approach is completely independent of spin adaption and hence a general scheme that can be applied to any UCC-VQE approach at any stage.

Note that in these simulations we did not take symmetry into account. If symmetry is taken into account, the classical minimization procedure can be further improved. Take LiH computed at HF/STO-3G as an example. The excitations including its SA-SAF-UCCSD ansatz are

$$\left\{ \tau_{0,0}^2, \tau_{0,0}^5, \tau_{1,1}^2, \tau_{1,1}^5, \tau_{0,1}^{2,5}, \tau_{0,7}^{2,11}, \tau_{0,7}^{2,8}, \tau_{0,7}^{3,9}, \tau_{0,7}^{4,10}, \tau_{0,7}^{5,11}, \tau_{0,6}^{2,11}, \tau_{1,7}^{2,11}, \tau_{0,6}^{2,8}, \tau_{0,6}^{3,9}, \tau_{0,6}^{4,10}, \tau_{0,6}^{5,11}, \tau_{1,7}^{2,8}, \tau_{1,7}^{3,9}, \tau_{1,7}^{4,10}, \tau_{1,7}^{5,11} \right\}, \quad (12)$$

where the orbital indices #0–#5 correspond to α spin orbitals with #0 and #1 occupied and others unoccupied and

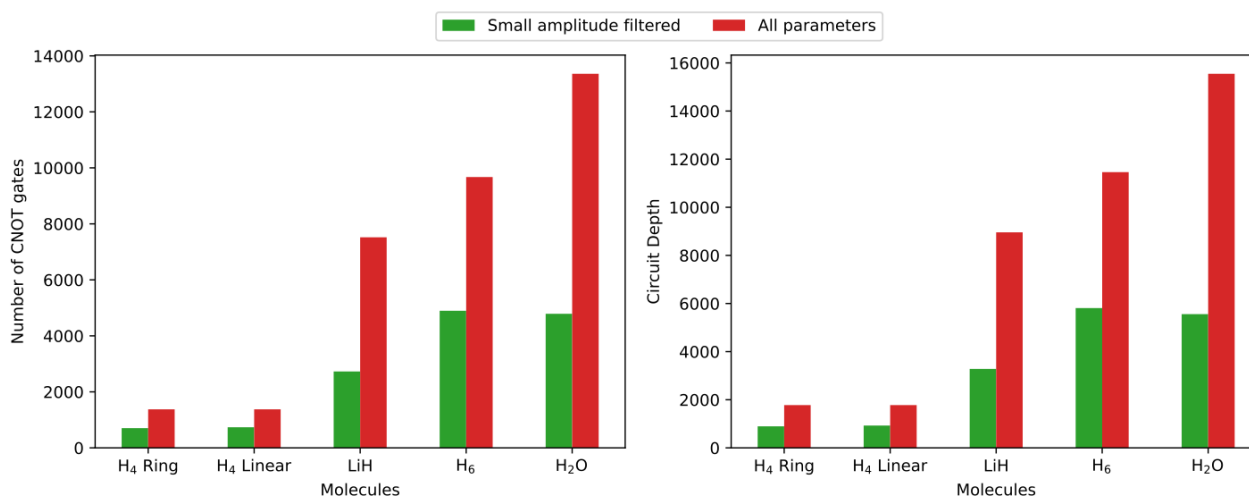


Figure 4. Number of CNOT gates and circuit depth of the UCCSD ansatz before and after small amplitude filtration (obtained through Qiskit inbuilt transpile functions).

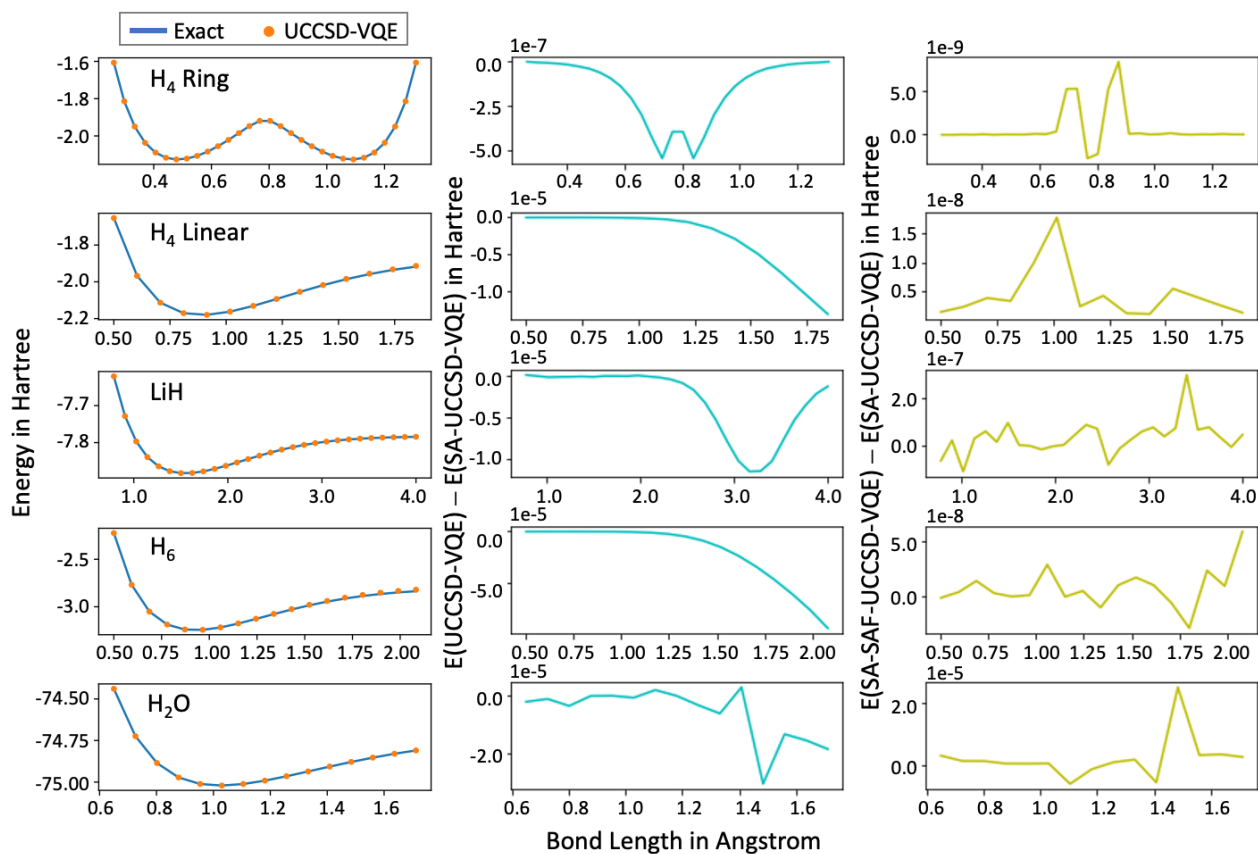


Figure 5. Potential energy surfaces of the five molecules computed by three UCCSD-VQE approaches. Left: the PES computed by conventional UCCSD-VQE and exact diagonalization. The exact results are same as the Full configuration interaction (FCI) results. Middle: the difference between the SA-UCCSD-VQE energies and the UCCSD-VQE energies for all five molecules at different bond lengths. Right: the difference between the SA-SAF-UCCSD-VQE energies and the SA-UCCSD-VQE energies for all five molecules at different bond lengths.

the indices #6–#11 correspond to β spin orbitals with #6 and #7 occupied and others unoccupied. Since the unoccupied π orbitals #3, #4, #9, and #10 are degenerate, the two sets $\{\tau_{0,7}^{3,9}, \tau_{0,6}^{3,9}, \tau_{1,7}^{3,9}\}$ and $\{\tau_{0,7}^{4,10}, \tau_{0,6}^{4,10}, \tau_{1,7}^{4,10}\}$ become interchangeable, and only one set needs to be optimized in the minimization procedure. Note that this treatment does not help reduce the load on the quantum computer since all the operators in (12) still need to be implemented on the quantum side to form the UCCSD ansatz.

C. Improvement through orbital selection

Selecting a portion of the orbitals in the UCC-VQE calculations while still maintaining the accuracy at a desired level not only reduces the number of free parameters but also reduces the number of qubits required to encode the problem on a quantum computer. In this section we use the H₂O molecule as an example to demonstrate the potential improvement in the computational efficiency brought by the entropy-based orbital selection. The computed single-orbital entropies of the H₂O molecule over the studied O–H bond length are shown in Figure 6a,b, from which several observations can be made.

- A qualitative agreement can be observed between the MP2 and CCSD entropy results, which yield the same orbital selections for the H₂O molecule over the entire range of bond lengths studied in this work. It is worth noting that in the strong correlation regime, even CCSD may be insufficient to provide accurate entropy results. Nevertheless, since our focus was on the relative "big" discrepancies (e.g., several orders of magnitude apart) of the entropy computed at the same theory level, orbital selection based on this qualitative entropy comparison works well for the tested cases. In more general cases, entropy can also be computed through other approximate approaches, e.g., a new approximate pair coefficient (APC) method was recently proposed³² for estimating single-site entropy, where the complex wave function is simplified in terms of a doubly occupied-virtual orbital pair interaction model.
- The entropies of orbitals #0 and #1 do not exhibit significant change over the entire bond length range. In particular, the entropies of orbital #0 are sufficiently small ($\sim 10^{-5}$) in comparison with the entropies of other orbitals (≥ 0.01).
- Regardless of the bond length, the entropies of orbitals #5 and #6 are always the largest in comparison with the entropies of other orbitals, and they keep increasing with the increasing bond length. Therefore, the entropy discrepancy (for example, between orbitals #5 (or #6) and #0) becomes larger with the increasing bond length.
- The entropy ordering of orbitals #2, #3, and #4 does not stay the same over the studied bond length range. Although the ordering exhibits crossovers over the entire bond length range, the smallest one is very

close to the entropy of orbital #0 (the discrepancy is < 0.01).

From these observations, since orbitals #0 and #2/#3/#4 become less important in contributing to the total correlation, they can be frozen from the original Hamiltonian. Specifically, (i) if the bond length $< 1.4 \text{ \AA}$, orbitals #0 and/or #4 can be frozen, (ii) if the bond length is between 1.4 \AA and 1.5 \AA , orbitals #0 and/or #3 can be frozen, and (iii) if the bond length $> 1.5 \text{ \AA}$, orbitals #0 and/or #2 can be frozen. Figure 6b compares the ground state energy of the Hamiltonian with and without freezing these orbitals through exact diagonalization. As can be seen, the error brought by freezing these orbitals is well below the chemical accuracy ($\sim 1.6 \times 10^{-3}$ a.u.), and the error gets smaller with the increasing bond length. In terms of improving the UCC-VQE efficiency, for the studied H₂O molecule, by removing one or two occupied orbitals, we reduce the number of qubits required from 14 to 12 or 10, respectively, and at the same time reduce the number of parameters in the UCCSD ansatz from 140 to 92 or 54, respectively. For larger molecular systems with larger basis sets, it has been reported that the entropy-based orbital selection is a robust approach for facilitating complete active space self-consistent field and/or quantum embedding calculations of relatively larger metal complex compounds, such as Ni(OH)₄ and Fe(II)-porphyrin complex^{32,33}. Running quantum simulations of the same systems would require 50 to 100 logical qubits, which necessitates a large amount of memory for performing emulation on classical computers. The memory constraint can be mitigated when running on real quantum machines, which, on the other hand, requires qubits and one/two-qubit gate operations with high fidelity that are still beyond the reach of current NISQ machines. However, if fault-tolerant quantum machines become available, the deployment of the studied UCCSD-VQE approaches will be straightforward.

IV. DISCUSSION

While the results described above demonstrate the efficiency of the approach proposed in this work, we are considering further improvement. For example, in the case of SA-SAF-UCCSD-VQE, the cutoffs, ϵ_1 , and ϵ_2 , and the heuristic number of iterations, κ , can be tweaked to balance the efficiency and accuracy. For example, Figure 7 examines different choices of κ on the efficiency of the SA-SAF-UCCSD-VQE approach compared to the conventional UCCSD-VQE and SA-UCCSD-VQE approaches. As shown, a slight increase in the κ value leads to a slightly longer time spent by the SA-SAF-UCCSD-VQE approach, but it is still significantly less than the conventional UCCSD-VQE and SA-UCCSD-VQE approaches. Note that for a given minimization task, κ determines the trade-off between the amount of time saved and the accuracy of the solution. For larger molecules or longer bond lengths, where the number of iterations might become substantial, choosing a large κ can still achieve significant cost reduction while maintaining good accuracy.

We can further speed up our approach by analyzing the

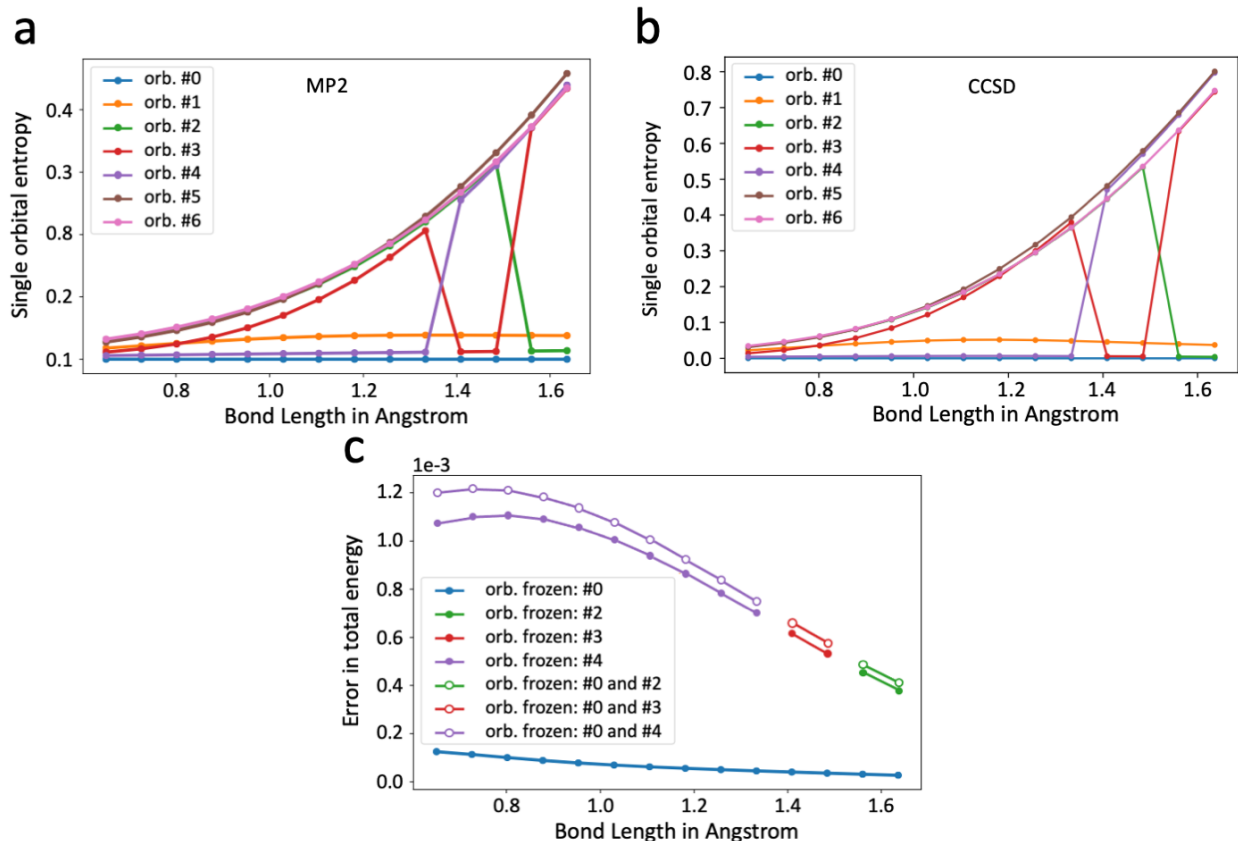


Figure 6. (a) Single orbital entropies of the H_2O molecule computed at the MP2/STO-3G level. (b) Single orbital entropies of the H_2O molecule computed at the CCSD/STO-3G level. (c) Error in energy induced by freezing the different orbitals.

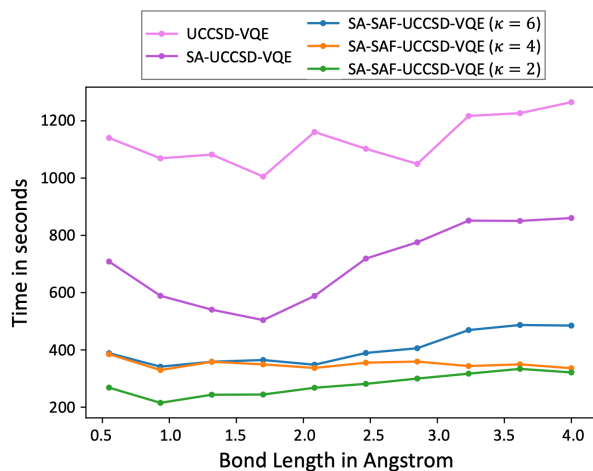


Figure 7. The time to convergence of UCCSD-VQE, SA-UCCSD-VQE, and SA-SAF-UCCSD-VQE with $\kappa = 2, 4, 6$ for LiH molecule at different bond lengths. the term “time” here refers to the actual amount of time taken by the UCCSD-VQE approaches employing a quantum emulator running on a classical machine.

relationship between the excitation parameters. For example, in Eq. (5), to implement spin adaption for the closed-shell electronic configuration, we have three choices: we can take any two of the three excitation coefficients to be

independent and write the third one as a function of the remaining two. In such a situation, if we apply small amplitude filtration after a spin adaption, the third parameter could be filtered out while the remaining two parameters, despite being close to each other, are minimized as independent parameters. Thus, we can perform small amplitude filtration before applying spin adaption. If the filtered parameters turn out to be one of the three quantities in Eq. (5), then only one of the remaining two could be explicitly included in the minimizer.

A more involved theoretical analysis could also be done to further reveal the connection between the parameters. Possible ways including employing the mutual information^{42–44} or evaluating the entropy of the wavefunction using the determinant amplitudes²⁶. For example, besides calculating the single-orbital entropies, we could also calculate two-orbital entropies from a 16×16 two-body reduced density matrix, where the trace would be taken over by all except two orbitals. Then, the mutual information could be calculated through

$$I_{i,j} = \frac{1}{2}(S_i + S_j - S_{ij}).$$

The value of the mutual information could be used in predicting possible dependencies among the parameters. A similar idea has been employed in the ADAPT-VQE algorithm⁴⁵ and could also be used for exploring the interconnection between the excitation operators involving more than two spatial orbitals.

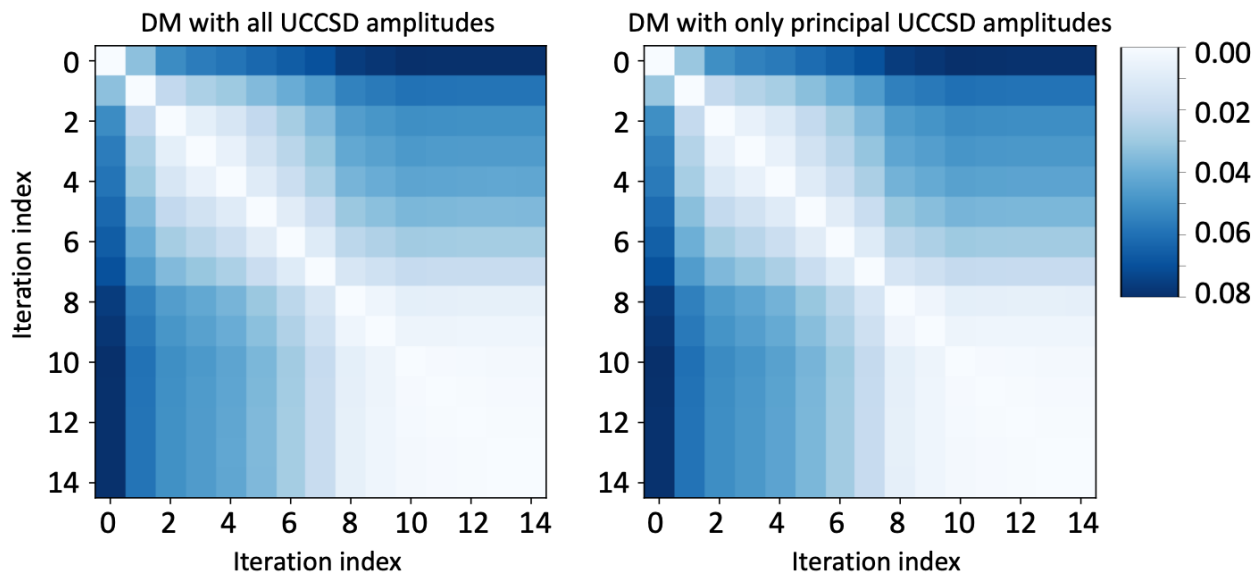
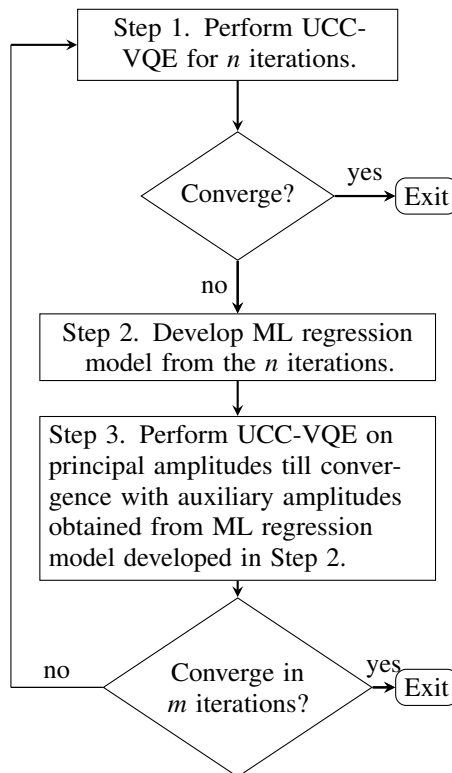


Figure 8. Distance matrix associated with the UCCSD-VQE iteration steps of LiH molecule. The distance matrix^{46,47} is defined as the norm of the amplitude difference between two iterations, representing the closeness of the amplitudes at different iterations.

Furthermore, one might anticipate the existence of other hidden relations among the remaining parameters. A way to explore such hidden relations has been reported recently (see Refs. 48,49), where it has been observed through phase analysis that the coupled-cluster amplitudes could be divided into principal and auxiliary categories and that a synergistic relationship between them exists during the iteration dynamics. Regarding the UCCSD ansatz, we conjecture that there is a similar significance of the principal amplitudes in the UCC-VQE iterations. Although obtaining a general and rigorous mathematical proof is more convoluted^{50,51}, a numerical phase space trajectory associated with the iterations can be straightforwardly observed for the test cases. For example, as shown in Figure 8, for LiH, the distance matrices computed with full UCCSD amplitudes and with only principal UCCSD amplitudes are nearly identical, indicating that the principal amplitudes can replicate the evolution exhibited by the full set of amplitudes.



Here, in Step 2 the ML regression model is developed through the following procedure

To find such a classification as well as the synergistic relationship, one could rely on some machine learning (ML) techniques. Here, as an exploratory attempt to proceed, we have prototyped an ML-assisted UCC-VQE approach, whose procedure can be summarized in the following flowchart.

1. Sorting the parameters in the n^{th} UCC-VQE iteration in descending order, and classify the parameters into principal and auxiliary amplitudes according to a predefined percentage p .
2. Using the labels in step 1 to collect the principal and auxiliary parameters from n iterations to form the subsets \mathbf{X} and \mathbf{Y} , respectively.

3. Treat subset \mathbf{X} as a set of independent variables and subset \mathbf{Y} as a set of dependent variables, and solve the regression problem $\mathcal{F} : \mathbf{X} \rightarrow \mathbf{Y}$.

If one is considering a linear regression model, then the regression model will be given by

$$\mathbf{Y} = \mathcal{F}(\mathbf{X}) = \mathbf{X} \cdot \beta, \quad (13)$$

and the ‘‘slope’’ β can be obtained by minimizing the cost function

$$\mathcal{C} = \|\mathbf{Y} - \mathcal{F}(\mathbf{X})\|_F^2 + \lambda \mathcal{R}(\beta) \quad (14)$$

through

$$\frac{\partial \mathcal{C}}{\partial \beta} = 0 \Rightarrow \beta = \mathbf{X}^T (\mathbf{X}\mathbf{X}^T + \lambda \mathbf{I})^{-1} \mathbf{Y}. \quad (15)$$

Here the subscript F denotes the Frobenius norm, and $\mathcal{R}(\beta)$ is a slope-dependent ridge term, which is added to enhance the robustness of the regression function on the test data. In the practical implementation, since the combination of Eqs. (13) and (15) includes only the so-called kernel term

$$\mathcal{K} = \mathbf{X}\mathbf{X}^T, \quad (16)$$

there is no need to explicitly compute β . To build a more general non-linear regression model, one can replace the kernel term by, for example, its polynomial form

$$\mathcal{K}(x_i, x_j) = (\gamma x_i x_j^T + c_0)^d, \quad (17)$$

where x_i is the i^{th} row vector of subset X , d is the order of the polynomial, and γ and c_0 are free parameters.

We have performed the ML-assisted SA-SAF-UCCSD-VQE simulation for the LiH molecule. The energy differences and the time to convergence compared with the non-ML SA-SAF-UCCSD-VQE simulations are given in Fig. 9. As can be seen, the energy differences between the ML and non-ML versions of the SA-SAF-UCCSD-VQE simulations are mostly on the order of 10^{-4} at most of the bond lengths. The time to convergence between the two versions at smaller bond lengths is comparable, but the ML-assisted simulation is clearly less time-consuming than the non-ML version at larger bond lengths (i.e., stronger correlation). We note that here we have explored a polynomial dependence of the auxiliary amplitudes on the principal ones in a heuristic manner. Other types of kernel functions could also be tested. Generally speaking, a kernel function that is more physically motivated would predict the relationship among the parameters more accurately.

The computational cost of the ML-assisted SA-SAF-UCCSD-VQE algorithm comes from two UCC-VQE iterations, as explained in Steps #1 and #3 in the algorithm above. One way to improve the efficiency of the algorithm, with a trade-off in accuracy, is to use a slightly greater iteration number m . For example, as shown in Figure 10, for $p = 30\%$ and $n = 4$ in the ML-assisted SA-SAF-UCCSD-VQE calculations of LiH molecule with different bond lengths, $m = 50$ helps the calculations quickly complete (in less than one minute) at all bond lengths, while the energy

difference with respect to the non-ML SA-SAF-UCCSD-VQE results increases by at least an order of magnitude, particularly when the bond length is greater than 3.0 \AA .

It is well-known that the performance of ML approaches depends on many factors, among which the size and/or quality of the training set is one of the most important. In Figure 10, we further compare the impact of the training set on the performance of ML-assisted SA-SAF-UCCSD-VQE calculations of the LiH molecule at different bond lengths. As can be seen, for all the choices of the training set, the time to convergence is not significantly impacted by a relatively slight change in the training set, and all are well below the time to convergence curve of the non-ML SA-SAF-UCCSD-VQE approach for all bond length values. On the other hand, accuracy is more sensitive to the choice of the training set. For example, the accuracy at bond lengths greater than 3.0 \AA when using $p = 30\%$ and $n = 4$ can be improved by increasing n from 4 to 7. In the latter setting (i.e., $p = 30\%$ and $n = 7$), the energy difference goes above the chemical accuracy only at two bond lengths around 3.0 \AA . One can continue expanding the size of the training set with $p = 40\%$ and $n = 4, 7$ to ensure the energy difference is well below the chemical accuracy at all bond lengths with $p = 40\%$ and $n = 7$ giving slightly better accuracy. Note that expanding the training set would also increase the time to convergence significantly at some point. For example, if n is increased to be greater than 11, the time to convergence will be close to that of the non-ML SA-SAF-UCCSD-VQE approach. Hence, an appropriate choice of p and n will lead to savings in both time and accuracy.

V. CONCLUSION AND OUTLOOK

In this work we have shown that the conventional UCC-VQE calculations can be improved significantly even after considering the spin adaption technique. The corresponding noise-free UCC-VQE simulations of some small molecules at various bond lengths show that a significant portion of cluster amplitudes are sufficiently small throughout the simulations, and these amplitudes can be identified heuristically from the first few UCC-VQE iterations. Thus, eliminating these amplitudes improves both quantum and classical calculations. Next, we proposed a way to freeze molecular orbitals based on their single-orbital entropy values calculated from a low-level theory such as MP2. Using the H_2O molecule as an example, we demonstrated that freezing the orbitals that have low enough entropy values compared with the rest can further simplify the ansatz with well-controlled error in energy. Furthermore, we explored the feasibility of employing some ML techniques for identifying other possible hidden relationships between the amplitudes. This work opens up some possible future directions. For example, one direction to explore is how to build a more appropriate, physically motivated kernel that, when combined with the right pair of principal and auxiliary amplitude subsets, would yield better results. Although we have used a single kernel here, the entire amplitude set could be divided into multiple principal and auxiliary amplitude subsets with a unique kernel for each pair of subsets. This might further improve UCC-VQE simulations, including the Adap-

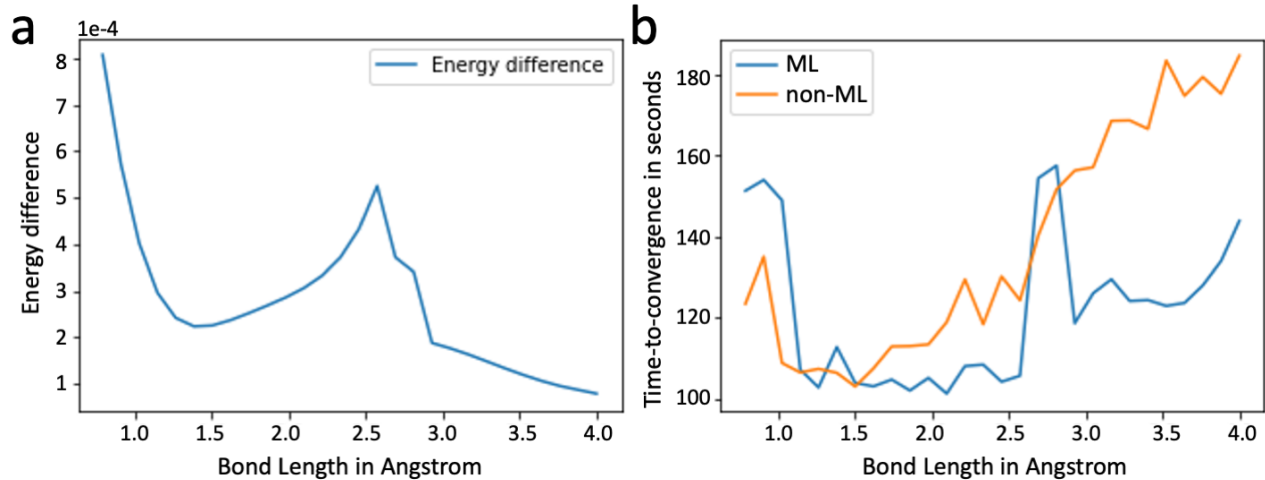


Figure 9. Efficiency of the ML-assisted SA-SAF-UCCSD-VQE simulations for the LiH molecule at different bond lengths in terms of (a) the energy difference and (b) the time-to-convergence in comparison with the non-ML SA-SAF-UCCSD-VQE simulations. In the ML-assisted simulations, $m = 1$, $n = 4$, and $\sim 30\% - 40\%$ of the total amplitudes are collected as principal amplitudes (i.e., $p = 30\%$ if bond length $< 2.8 \text{ \AA}$, and $p = 40\%$ otherwise) for the construction of a nonlinear regression model employing Eq. (17) as the kernel with $\gamma = 1$, $c_0 = 0$, and $d = 3$.

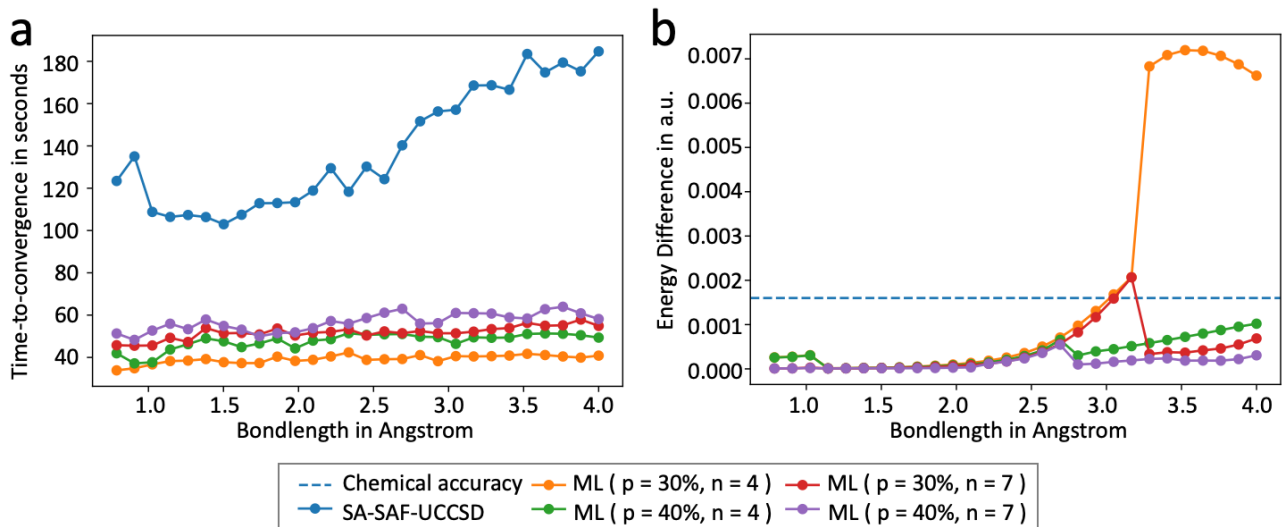


Figure 10. The impact of the training set on (a) the time to convergence and (b) the accuracy of the ML-assisted SA-SAF-UCCSD-VQE simulations for the LiH molecule at different bond lengths is investigated. In the ML-assisted simulations at each bond length, $m = 50$, and two percentages of the principal amplitudes, $p = 30\%$ and 40% , with $n = 4$ and 7 SA-SAF-UCCSD-VQE iterations, respectively, are taken to construct a nonlinear regression model. This model employs Eq. (17) as the kernel with $\gamma = 3$, $c_0 = 1$, and $d = 3$.

tive Derivative-Assembled Pseudo-Trotter (ADAPT) ansatz VQE²², pulse level VQE⁵², and several methods for excited states and properties on top of VQEs (e.g., the quantum self-consistent equation-of-motion⁵³). Additionally, since VQEs usually target a small active space, the entropy-based active space selection can also be employed to facilitate the downfolding methods that have been developed to treat the remaining dynamical correlation^{54–56}.

Finally, it's worth emphasizing that our work aims to reduce the number of parameters used to optimize and prepare the UCCSD ansatz in hybrid classical-quantum computation. The parameter reduction brought by some techniques used in our work (such as small amplitude filtration and entropy-based orbital selection) will further reduce

the circuit depth required to prepare the UCCSD ansatz. Given the current NISQ quantum hardware, deeper circuits will usually be more influenced by noise. From this perspective, our simulations, though noise-free, are still very useful since it guarantees better performance than the conventional UCCSD ansatz due to its relatively shallow circuit depth while maintaining the same accuracy level. Also, the techniques discussed in our work can also be combined with other coupled cluster or post-Hartree-Fock approaches. Regarding the scalability of our proposed techniques, reduced-scaling coupled cluster approaches have been well-developed on the classical computing side (see Ref. 57 for a recent review), and parallel quantum computing techniques such as clusterVQE⁵⁸ and measurement

tapering⁵⁹ have been developed on the quantum side. All these techniques can be combined with the discussed techniques in this work to improve scalability.

ACKNOWLEDGMENT

This material is based upon work supported by the U.S. Department of Energy, Office of Science, and National Quantum Information Science Research Centers. Y.A. acknowledges support from the U.S. Department of Energy, Office of Science, under contract DE-AC02-06CH11357 at Argonne National Laboratory. The demonstration of our proposal approaches can be obtained from <https://github.com/Shashank-G-M/Parameter-redundancy-VQE>

REFERENCES

- Alberto Peruzzo, Jarrod McClean, Peter Shadbolt, Man-Hong Yung, Xiao-Qi Zhou, Peter J. Love, Alán Aspuru-Guzik, and Jeremy L. O’Brien. A variational eigenvalue solver on a photonic quantum processor. *Nat. Commun.*, 5(1):4213, 2014.
- Sourav Pal. Use of a unitary wavefunction in the calculation of static electronic properties. *Theor. Chim. Acta*, 66(3-4):207–215, 1984.
- Chiranjib Sur, Rajat K Chaudhuri, Bijaya K Sahoo, BP Das, and D Mukherjee. Relativistic unitary coupled cluster theory and applications. *J. Phys. B*, 41(6):065001, 2008.
- Bridgette Cooper and Peter J Knowles. Benchmark studies of variational, unitary and extended coupled cluster methods. *J. Chem. Phys.*, 133(23):234102, 2010.
- Rodney J. Bartlett, Stanislaw A. Kucharski, and Jozef Noga. Alternative coupled-cluster ansätze II. the unitary coupled-cluster method. *Chem. Phys. Lett.*, 155(1):133–140, 1989.
- Andrew G Taube and Rodney J Bartlett. New perspectives on unitary coupled-cluster theory. *Int. J. Quantum Chem.*, 106(15):3393–3401, 2006.
- Mark R Hoffmann and Jack Simons. A unitary multiconfigurational coupled-cluster method: Theory and applications. *J. Chem. Phys.*, 88(2):993–1002, 1988.
- Werner Kutzelnigg. Error analysis and improvements of coupled-cluster theory. *Theor. Chim. Acta*, 80(4-5):349–386, 1991.
- Francesco A Evangelista, Garnet Kin-Lic Chan, and Gustavo E Scuseria. Exact parameterization of fermionic wave functions via unitary coupled cluster theory. *J. Chem. Phys.*, 151(24):244112, 2019.
- Abhinav Anand, Philipp Schleich, Sumner Alperin-Lea, Phillip WK Jensen, Sukin Sim, Manuel Díaz-Tinoco, Jakob S Kottmann, Matthias Degroote, Artur F Izmaylov, and Alán Aspuru-Guzik. A quantum computing view on unitary coupled cluster theory. *Chem. Soc. Rev.*, 2022.
- Michael Kühn, Sebastian Zanker, Peter Deglmann, Michael Marthaler, and Horst Weiß. Accuracy and resource estimations for quantum chemistry on a near-term quantum computer. *J. Chem. Theory Comput.*, 15(9):4764–4780, 2019.
- D.A. Fedorov, B. Peng, N. Govind, and Y. Alexeev. VQE method: a short survey and recent developments. *Mater. Theory*, 6:2, 2022.
- Jules Tilly, Hongxiang Chen, Shuxiang Cao, Dario Picozzi, Kanav Setia, Ying Li, Edward Grant, Leonard Wossnig, Ivan Rungger, George H. Booth, and Jonathan Tennyson. The variational quantum eigensolver: A review of methods and best practices. *Phys. Rep.*, 986:1–128, 2022.
- Abhinav Kandala, Antonio Mezzacapo, Kristan Temme, Maika Takita, Markus Brink, Jerry M. Chow, and Jay M. Gambetta. Hardware-efficient variational quantum eigensolver for small molecules and quantum magnets. *Nature*, 549(7671):242–246, 2017.
- Abhinav Kandala, Kristan Temme, Antonio D. Córcoles, Antonio Mezzacapo, Jerry M. Chow, and Jay M. Gambetta. Error mitigation extends the computational reach of a noisy quantum processor. *Nature*, 567(7749):491–495, 2019.
- Jarrod R. McClean, Sergio Boixo, Vadim N. Smelyanskiy, Ryan Babush, and Hartmut Neven. Barren plateaus in quantum neural network training landscapes. *Nat. Commun.*, 9(1):4812, 2018.
- Joonho Lee, William J Huggins, Martin Head-Gordon, and K Birgitta Whaley. Generalized unitary coupled cluster wave functions for quantum computation. *J. Chem. Theory Comput.*, 15(1):311–324, 2018.
- Wataru Mizukami, Kosuke Mitarai, Yuya O. Nakagawa, Takahiro Yamamoto, Tennin Yan, and Yu-ya Ohnishi. Orbital optimized unitary coupled cluster theory for quantum computer. *Phys. Rev. Research*, 2:033421, Sep 2020.
- Mekena Metcalf, Nicholas P. Bauman, Karol Kowalski, and Wibe A. de Jong. Resource-efficient chemistry on quantum computers with the variational quantum eigensolver and the double unitary coupled-cluster approach. *J. Chem. Theory Comput.*, 16(10):6165–6175, 2020. PMID: 32915568.
- Karol Kowalski. Properties of coupled-cluster equations originating in excitation sub-algebras. *J. Chem. Phys.*, 148(9):094104, 2018.
- Ilya G. Ryabinkin, Tzu-Ching Yen, Scott N. Genin, and Artur F. Izmaylov. Qubit coupled cluster method: A systematic approach to quantum chemistry on a quantum computer. *J. Chem. Theory Comput.*, 14(12):6317–6326, 2018.
- Harper R. Grimsley, Sophia E. Economou, Edwin Barnes, and Nicholas J. Mayhall. An adaptive variational algorithm for exact molecular simulations on a quantum computer. *Nat. Commun.*, 10(1):3007, dec 2019.
- Y. S. Yordanov, V. Armaos, C. H. W. Barnes, and D. R. M. Arvidsson-Shukur. Qubit-excitation-based adaptive variational quantum eigensolver. *Commun. Phys.*, 4:228, 2021.
- Ilya G. Ryabinkin, Robert A. Lang, Scott N. Genin, and Artur F. Izmaylov. Iterative qubit coupled cluster approach with efficient screening of generators. *J. Chem. Theory Comput.*, 16(2):1055–1063, 2020.
- Dmitry A. Fedorov, Yuri Alexeev, Stephen K. Gray, and Matthew Otten. Unitary selective coupled cluster method. *Quantum*, 6:703, May 2022.
- J. Wayne Mullinax and Norm M. Tubman. Large-scale sparse wavefunction circuit simulator for applications with the variational quantum eigensolver, 2023.
- Josef Paldus. Correlation problems in atomic and molecular systems, V: Spin-adapted coupled cluster many-electron theory. *J. Chem. Phys.*, 67(1):303–318, 1977.
- Gustavo E Scuseria, Andrew C Scheiner, Timothy J Lee, Julia E Rice, and Henry F Schaefer III. The closed-shell coupled cluster single and double excitation (CCSD) model for the description of electron correlation. a comparison with configuration interaction (CISD) results. *J. Chem. Phys.*, 86(5):2881–2890, 1987.
- Takashi Tsuchimochi, Yuto Mori, and Seiichiro L. Ten-no. Spin-projection for quantum computation: A low-depth approach to strong correlation. *Phys. Rev. Research*, 2:043142, Oct 2020.
- Katharina Boguslawski and Paweł Tecmer. Orbital entanglement in quantum chemistry. *Int. J. Quantum Chem.*, 115(19):1289–1295, 2015.
- Katharina Boguslawski, Paweł Tecmer, Gergely Barcza, Örs Legeza, and Markus Reiher. Orbital entanglement in bond-formation processes. *J. Chem. Theory Comput.*, 9(7):2959–973, 2013.
- Pavlo Golub, Andrej Antalik, Libor Veis, and Jiri Brabec. Machine learning-assisted selection of active spaces for strongly correlated transition metal systems. *J. Chem. Theory Comput.*, 17(10):6053–6072, 2021.
- Jonathan M. Waldrop, Theresa L. Windus, and Niranjan Govind. Projector-based quantum embedding for molecular systems: An investigation of three partitioning approaches. *J. Phys. Chem. A*, 125(29):6384–6393, 2021.
- Qiskit: An open-source framework for quantum computing, 2021.
- Pauli Virtanen, Ralf Gommers, Travis E. Oliphant, Matt Haberland, Tyler Reddy, David Cournapeau, Evgeni Burovski, Pearu Peterson, Warren Weckesser, Jonathan Bright, Stéfan J. van der Walt, Matthew Brett, Joshua Wilson, K. Jarrod Millman, Nikolay Mayorov, Andrew R. J. Nelson, Eric Jones, Robert Kern, Eric Larson, C J Carey, İlhan Polat, Yu Feng, Eric W. Moore, Jake VanderPlas, Denis Laxalde, Joseph Perktold, Robert Cimrman, Ian Henriksen, E. A. Quintero, Charles R. Harris, Anne M. Archibald, Antônio H. Ribeiro, Fabian Pedregosa, Paul van Mulbregt, and SciPy 1.0 Contributors. SciPy 1.0: Fundamental Algorithms for Scientific Computing in Python. *Nature Methods*, 17:261–272, 2020.

- ³⁶P. Jordan and E. Wigner. Über das paulische Äquivalenzverbot. *Z. Physik*, 47:631–651, 1928.
- ³⁷Ian D. Kivlichan, Jarrod McClean, Nathan Wiebe, Craig Gidney, Alán Aspuru-Guzik, Garnet Kin-Lic Chan, and Ryan Babbush. Quantum simulation of electronic structure with linear depth and connectivity. *Phys. Rev. Lett.*, 120:110501, Mar 2018.
- ³⁸Iordanis Kerenidis, Jonas Landman, and Natansh Mathur. Classical and quantum algorithms for orthogonal neural networks, 2022.
- ³⁹Yordan S. Yordanov, David R. M. Arvidsson-Shukur, and Crispin H. W. Barnes. Efficient quantum circuits for quantum computational chemistry. *Phys. Rev. A*, 102:062612, Dec 2020.
- ⁴⁰Ilias Magoulas and Francesco A. Evangelista. Cnot-efficient circuits for arbitrary rank many-body fermionic and qubit excitations. *J. Chem. Theory Comput.*, 19(3):822–836, 2023.
- ⁴¹Frank Verstraete, J. Ignacio Cirac, and José I. Latorre. Quantum circuits for strongly correlated quantum systems. *Phys. Rev. A*, 79:032316, Mar 2009.
- ⁴²Luigi Amico, Rosario Fazio, Andreas Osterloh, and Vlatko Vedral. Entanglement in many-body systems. *Rev. Mod. Phys.*, 80:517–576, May 2008.
- ⁴³Jörg Rissler, Reinhard M. Noack, and Steven R. White. Measuring orbital interaction using quantum information theory. *Chem. Phys.*, 323(2):519–531, 2006.
- ⁴⁴Zhen Huang and Sabre Kais. Entanglement as measure of electron–electron correlation in quantum chemistry calculations. *Chem. Phys. Lett.*, 413(1):1–5, 2005.
- ⁴⁵Zi-Jian Zhang, Thi Ha Kyaw, Jakob S Kottmann, Matthias Degroote, and Alán Aspuru-Guzik. Mutual information-assisted adaptive variational quantum eigensolver. *Quantum Sci. Technol.*, 6(3):035001, aug 2021.
- ⁴⁶J.-P. Eckmann, S. Oliffson Kamphorst, and D. Ruelle. Recurrence plots of dynamical systems. *Europhys. Lett.*, 4(9):973, nov 1987.
- ⁴⁷Norbert Marwan, M. Carmen Romano, Marco Thiel, and Jürgen Kurths. Recurrence plots for the analysis of complex systems. *Phys. Rep.*, 438(5):237–329, 2007.
- ⁴⁸Valay Agarawal, Samrendra Roy, Anish Chakraborty, and Rahul Maitra. Accelerating coupled cluster calculations with nonlinear dynamics and supervised machine learning. *J. Chem. Phys.*, 154(4):044110, 2021.
- ⁴⁹Valay Agarawal, Samrendra Roy, Kapil K Shrawankar, Mayank Ghogale, S Bharathi, Anchal Yadav, and Rahul Maitra. A hybrid coupled cluster–machine learning algorithm: Development of various regression models and benchmark applications. *J. Chem. Phys.*, 156(1):014109, 2022.
- ⁵⁰Valay Agarawal, Chayan Patra, and Rahul Maitra. An approximate coupled cluster theory via nonlinear dynamics and synergetics: The adiabatic decoupling conditions. *J. Chem. Phys.*, 155(12):124115, 2021.
- ⁵¹Chayan Patra, Valay Agarawal, Dipanjali Halder, Anish Chakraborty, Dibyendu Mondal, Sonaldeep Halder, and Rahul Maitra. A synergistic approach towards optimization of coupled cluster amplitudes by exploiting dynamical hierarchy. *Chem. Phys. Chem.*, 24(4):e202200633, 2023.
- ⁵²O.R. Meitei, B.T. Gard, G.S. Barron, D.P. Pappas, S.E. Economou, E. Barnes, and N.J. Mayhall. Gate-free state preparation for fast variational quantum eigensolver simulations. *npj Quantum Inf.*, 7:155, 2021.
- ⁵³Ayush Asthana, Ashutosh Kumar, Vibin Abraham, Harper Grimsley, Yu Zhang, Lukasz Cincio, Sergei Tretiak, Pavel A. Dub, Sophia E. Economou, Edwin Barnes, and Nicholas J. Mayhall. Quantum self-consistent equation-of-motion method for computing molecular excitation energies, ionization potentials, and electron affinities on a quantum computer. *Chem. Sci.*, 14:2405–2418, 2023.
- ⁵⁴Renke Huang, Chenyang Li, and Francesco A. Evangelista. Leveraging small scale quantum computers with unitarily downfolded hamiltonians, 2022.
- ⁵⁵Nicholas P Bauman, Eric J Bylaska, Sriram Krishnamoorthy, Guang Hao Low, Nathan Wiebe, Christopher E Granade, Martin Roetteler, Matthias Troyer, and Karol Kowalski. Downfolding of many-body hamiltonians using active-space models: Extension of the sub-system embedding sub-algebras approach to unitary coupled cluster formalisms. *J. Chem. Phys.*, 151(1):014107, 2019.
- ⁵⁶Karol Kowalski and Nicholas P. Bauman. Sub-system quantum dynamics using coupled cluster downfolding techniques. *J. Chem. Phys.*, 152(24):244127, 2020.
- ⁵⁷T. Daniel Crawford, Ashutosh Kumar, Alexandre P. Bazanté, and Roberto Di Remigio. Reduced-scaling coupled cluster response theory: Challenges and opportunities. *WIREs Computational Molecular Science*, 9(4):e1406, 2019.
- ⁵⁸Y. Zhang, L. Cincio, C.F.A. Negre, P. Czarnik, P.J. Coles, P.M. Anisimov, S.M. Mniszewski, S. Tretiak, and P.A. Dub. Variational quantum eigensolver with reduced circuit complexity. *npj Quantum Inf.*, 8:96, 2022.
- ⁵⁹Daniel Claudino, Bo Peng, Karol Kowalski, and Travis S. Humble. Modeling singlet fission on a quantum computer, 2023.

